Tunable Spin Transport and Spin-dependent Seebeck Effect in Boron-based Two-dimensional MBene Transition Metal Compounds

Cuicui Sun [a], Yuxiu Wang [b*], Haocheng Zhang [a], Yue Sun [a], Zhongteng Liu [a], Xuanchen Zhou[a], Guiling Zhang [c*]

[a] School of Civil Engineering, Shandong Jiaotong University, Jinan 250300, China

[b] School of Ecology and Environment, Yuzhang Normal University, Nanchang 330103, China

[c] School of Material Science and Chemical Engineering, Harbin University of Science and Technology, Harbin 150080, China

The principle of thermal spin related transport properties

Within the nonequilibrium Green's function methods, one can calculate the spin-dependent current by using the Landauer-Büttiker formalism[1]

$$I^{\uparrow/\downarrow} = \frac{e}{h}\int_{-\infty}^{\infty}\left\{T^{\uparrow/\downarrow}\left[f_L(\varepsilon,T_L) - f_R(\varepsilon,T_R)\right]\right\}d\varepsilon \quad (1)$$

where e is the electron charge, h is the plank constant, $f_{L/R}$ (ε T) is the equilibrium Fermi-Dirac distribution for the left (right) electrode under $\mu_{L/R}$, $f_{L/R}(\varepsilon,T_{L/R}) = \frac{1}{1+e^{\left(\frac{E-\mu_{L/R}}{k_B T_{L/R}}\right)}}$, $T_{L/R}$ is the temperature of the left (right) contract, and $T^{\uparrow/\downarrow}$ is the spin resolved transmittance function and can be defined as

$$T^{\uparrow/\downarrow} = Tr\left[\Gamma_L(\varepsilon)G^{R}_{\uparrow/\downarrow}\Gamma_R(\epsilon)G^{A}_{\uparrow/\downarrow}\right] \quad (2)$$

where $G^{R/A}_{\uparrow/\downarrow}$ is the spin-resolved retarded (advanced) Green's functions of the central region and $\Gamma_{L/R}(\varepsilon)$is the coupling matrix of the left (right) contact.

The spin-dependent Seebeck coefficient $S_{\uparrow/\downarrow}$ can be denoted by[2, 3]

$$S_{\uparrow/\downarrow} = -\frac{1}{|e|T}\frac{L_{1,\uparrow/\downarrow}}{L_{0,\uparrow/\downarrow}} \quad (3)$$

where $L_{1,\uparrow/\downarrow}$ is defined as an intermediary function:

$$L_{n,\uparrow/\downarrow} = -\frac{1}{h}\int_{-\infty}^{\infty} d\varepsilon(\varepsilon-\mu)^n \frac{\partial f}{\partial \varepsilon} T_{\uparrow/\downarrow}(\varepsilon) \tag{4}$$

the spin-dependent conductance is $\sigma_{\uparrow/\downarrow} = e^2 L_{0,\uparrow/\downarrow}$. Subsequently, $\sigma_{ch} = \sigma_{\uparrow} + \sigma_{\downarrow}$ and $\sigma_{sp} = |\sigma_{\uparrow} - \sigma_{\downarrow}|$ can be used to compute the charge conductance (σ_{ch}) and spin conductance (σ_{sp}), respectively.

The thermal conductance of electrons is $\kappa_e = \kappa_{e\uparrow} + \kappa_{e\downarrow}$[4], $\kappa_{e(\uparrow/\downarrow)}$ is thermal conductance of spin-up(spin-down) electrons.

$$\kappa_{e\uparrow/\downarrow}(\mu,T) = \frac{1}{T}\left\{L_{2,\uparrow/\downarrow}(\mu,T) - \frac{\left[L_{1,\uparrow/\downarrow}(\mu,T)\right]^2}{L_{0,\uparrow/\downarrow}(\mu,T)}\right\} \tag{5}$$

Based on the theory of Caroli, the phonon transmission function $T_{ph}(\omega)$ is as follows[5, 6]

$$T_{ph}(\omega) = Tr\left[\Gamma_L(\omega) G_C^R(\omega) \Gamma_R G_C^A(\omega)\right] \tag{6}$$

where $G_C^{R/A}$ is the retarded/advanced Green's function of the device, and $\Gamma_{L/R}$ describes the broaden function. And G_C^R and G_C^A satisfy the relationship $G_C^R = G_C^{A\dagger}$.

Here $G_C^R = [(\omega + i\eta)^2 M - K_C - \sum_L^r(\omega) - \sum_R^r(\omega)]^{-1}$, K_C is the dynamical matrix, M is the diagonal matrix with the element corresponding to the masses of the atoms, ω stands for phonon frequency, and $\sum_{L/R}^r$, indicates the self-energy of the left/right electrode.

The phonon thermal conductance (κ_{ph}) can be calculated using[7]

$$\kappa_{ph} == \frac{\hbar}{2\pi}\int_{-\infty}^{\infty} T_{ph}(\omega) \frac{\partial f_B(\omega,T)}{\partial T} \omega d\omega \tag{7}$$

where $T_{ph}(\omega)$ is the phonon transmission function, $f_B(\omega,T)$ is the Bose–Einstein distribution function of the phonon, and T is the device average temperature.

Finally, the charge figure of merit (ZT_{ch}) and spin figure of merit (ZT_{sp}) are specified as[8]

$$ZT_{ch/sp} = \frac{S_{ch/sp}^{2}\sigma_{ch/sp}T}{\kappa_{e(\uparrow)} + \kappa_{e(\downarrow)} + \kappa_{ph}} \quad (8)$$

where charge Seebeck coefficient $S_{ch} = (S_{\uparrow}+S_{\downarrow})/2$, and spin Seebeck coefficient $S_{sp} = S_{\uparrow}-S_{\downarrow}$.

The Stoner criterion (ST) was calculated to evaluate the itinerant magnetism from M in the M_2B (M = Sc, Ti, and V) monolayers. Stoner criterion is defined as ST= $I \times D(E_F)$. Where $D(E_F)$ is the density of states (DOS) of all *d* orbitals of M at the Fermi level for non-spin-polarized M_2B (M = Sc, Ti, and V) (Fig. S1). For M_2B (M = Sc, Ti, and V), $D(E_F)$ 1.71, 1.89, and 4.74 state/eV for Sc_2B, Ti_2B, and V_2B, respectively.

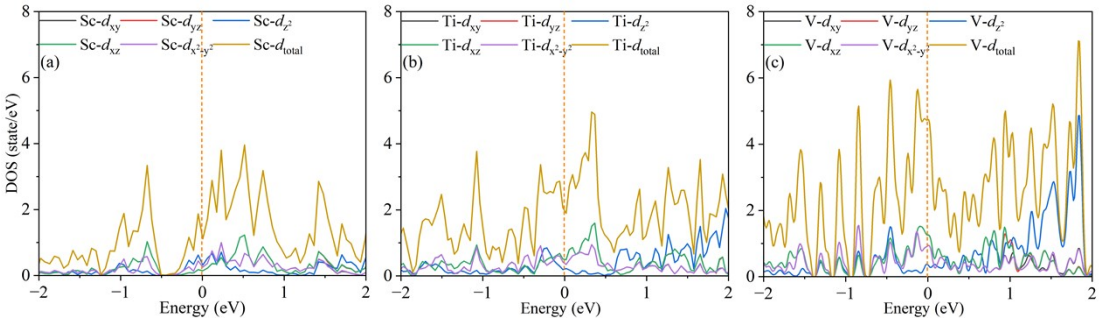

Fig. S1 PDOS of the M *d* orbitals in M_2B (M = Sc, Ti, and V) bulk systems.

The calculated DOS of all *d* orbitals of M at the Fermi level for non-spin-polarized M_2B D (E_F), Stoner parameter I, the average value of the splitting between the corresponding spin-up and spin-down bands around Fermi level $\langle\epsilon\rangle_k$ and the Stoner criterion ST = $I \times D(E_F)$ are listed in Table S1. Here, the $\langle\epsilon\rangle_k = I \times m$, and the m is the average value of the magnetic moments on M atoms.

Table S1 Parameters in the Stoner model.

	$D(E_F)$	I	$\langle\epsilon\rangle_k$	$I \times D(E_F)$
Sc_2B	1.71	0.46	0.46	0.79
Ti_2B	1.89	0.58	1.25	1.10
V_2B	4.74	0.51	0.64	2.42

When a bias voltage V_b is applied in the system, the chemical potential of the electrodes is $\mu_{L(R)} = E_F \pm eV_b/2$. According to

$$I^{\uparrow/\downarrow} = \frac{e}{h}\int_{-\infty}^{\infty}\{T^{\uparrow/\downarrow}[f_L(\varepsilon,T_L) - f_R(\varepsilon,T_R)]\}d\varepsilon$$, the spin-dependent current is proportional to the integration of the transmission coefficient within the bias-dependent energy range (E_F-V_b/2, E_F+V_b/2), which is called the bias window. Only the transport coefficients entering the bias window are contributable to the currents. In the PM configuration, there are a large number of spin up transmission peaks in the bias window, with high transmission coefficients and symmetric evolution within the bias voltage range of (-1.0 V, 1.0 V) for the Sc_2B and Ti_2B. Therefore, as mentioned above, the spin up current increases with the increase of bias voltage, as shown in Fig. S2. Correspondingly, there are fewer spin down transmission peaks within the bias window, resulting in lower spin down currents. The results indicate that spin filtering effects independent of bias direction occur in the P configuration. On the contrary, for V_2B, spin down is greater than spin up, but spin filtering effect also exists.

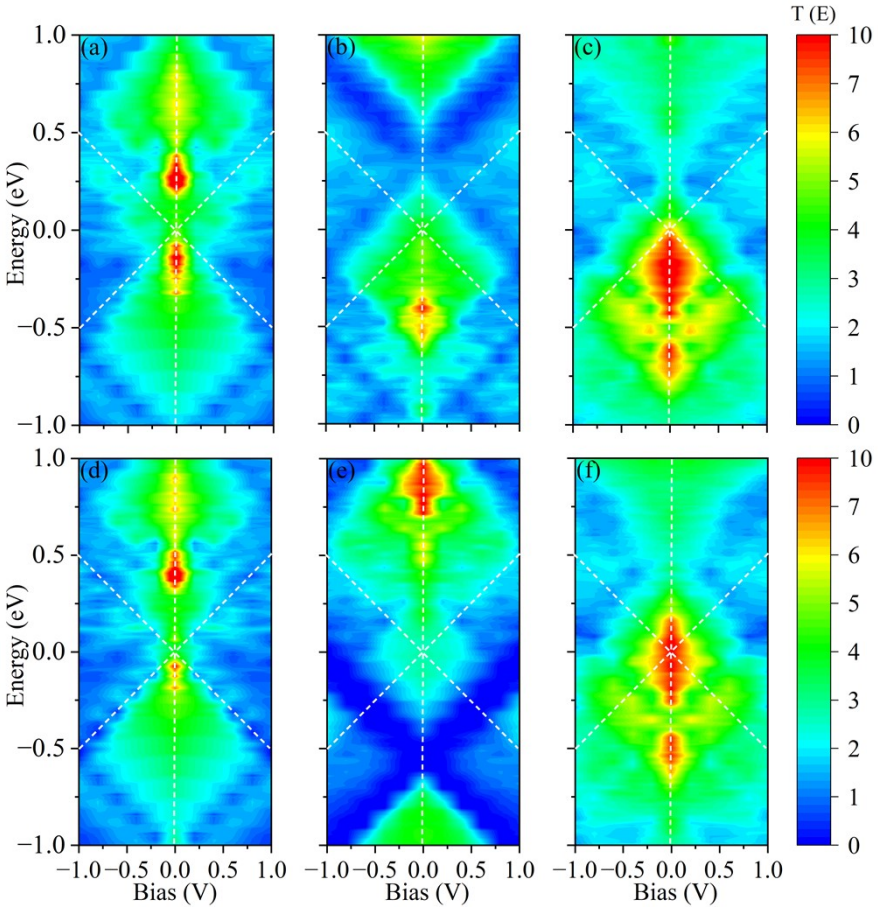

Fig. S2 Contour maps of (a)−(c) spin-up and (d)−(f) spin-down bias-voltage-dependent transmission spectra for the PM configuration of M_2B device. (a, d) Sc_2B, (b, e) Ti_2B,

and (c, f) V_2B. The white dash lines designate the region of the bias window and E_F.

The spin rectification ratio, which characterizes the level of spin rectification, was calculated using the formula $RR = I_{-V} / I_{+V}$, where the I_{-V} and I_V are the total currents under negative and positive bias voltages, respectively. Clearly, the RR in the PM field is almost negligible, as displayed in Fig. S3.

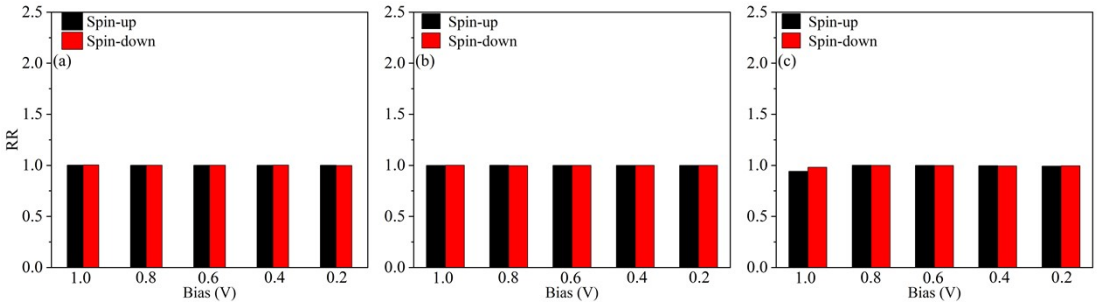

Fig. S3 The spin rectification ratio of the M_2B device under the PM field. (a) Sc_2B, (b) Ti_2B, and (c) V_2B.

The DOS of the left electrode and right electrode along with the transmission spectra at -0.8 V and 0.8 V bias voltages of Ti_2B were illustrated in Fig. S4 to understand the spin current rectification mechanism. When the spin-up and spin-down PDOS peaks of the left and right electrode can match each other well, there will be very large spin-up and spin-down currents originating from a large transmission coefficient. In the PM configuration, the overlap of the spin-up DOS between the two electrodes is greater than that of the spin-down DOS, leading to a significant spin-up transmission peak within the bias window (−0.4 V to 0.4 V), which results in a larger spin-up current regardless of 0.8 V or −0.8 V and explains the SFE in the PM configuration, as shown in Fig. S4(a, b). In the APM configuration, within the −0.8 V bias window, the spin-up DOS overlap is greater than that the spin-down, resulting in a smaller spin-down current compared to spin-up. In contrast, for the +0.8 V bias window, the opposite occurs, explaining the dual spin-filtering effect observed in the APM configuration, as shown in Fig. S4(c, d).

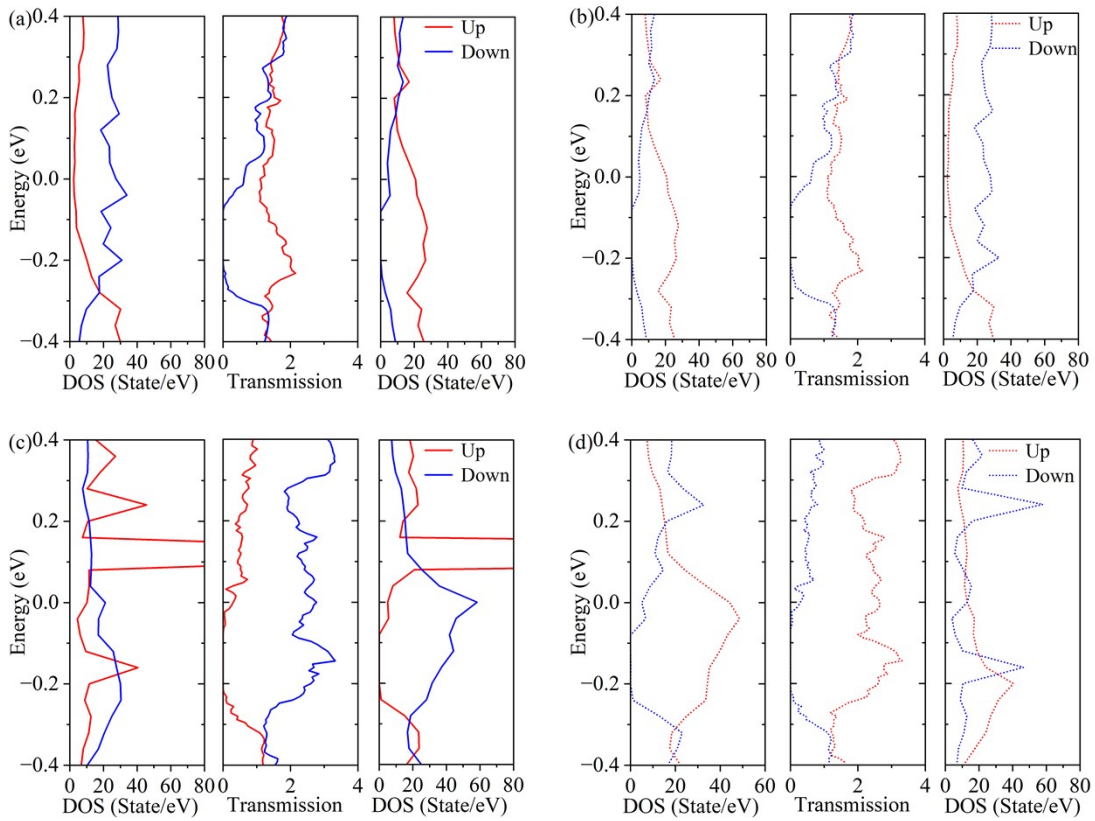

Fig. S4 The spin-resolved DOS spectra of the left electrode and right electrode along with the transmission spectrum of the Ti_2B device, (a) PM configuration at 0.8 V, (b) PM configuration at −0.8 V, (c) APM configuration at 0.8 V, and (d) APM configuration at −0.8 V.

Since the contacts of the left (higher temperature) and right (lower temperature) leads are the same material and have the similar density of states (DOS), the difference in carrier concentrations between the left and the right leads is determined by the Fermi distribution ($f_L(E,T_L) - f_R(E,T_R)$), which is intimately related to the electron temperatures at the two terminals. It is clearly demonstrated that carriers (electron) with energy higher than the Fermi energy flow from the left (higher temperature) to the right (lower temperature), giving rise to electron current I_e, because the electron distribution of the left is higher than that of the right. Conversely, carriers (hole) with energy lower than the Fermi energy flow in the opposite directions, resulting in hole current I_h. If the transmission spectra are symmetric, I_e and I_h will cancel out each other, leading to zero net thermal current. The transmission spectra in our systems are energy-dependent and asymmetric, as shown in Fig. S5. Therefore, spin splitting occurs and results in a nonzero thermally driven spin current.

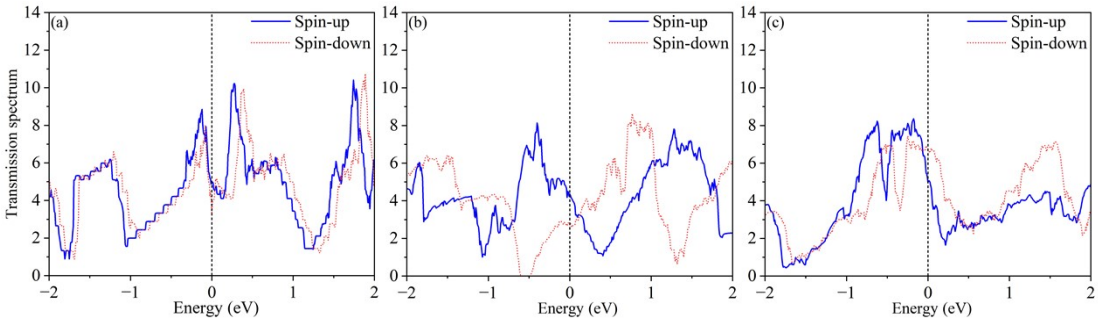

Fig. S5 The spin-dependent transmission spectrums of the Sc_2B, Ti_2B and V_2B, respectively, without temperature difference and applied bias voltage.

The current spectra J(E) of spin-up electrons for different temperature settings are shown in Fig. S6, where the area covered under the curves associated with the axis of J = 0 reveals the magnitude of the spin currents. Clearly, the current spectra J(E) increase with rising temperature, as shown in Fig. S4. From 100 K to 400 K, although the peak value of J(E) decreases, the width of the peak increases significantly, indicating a larger spin current.

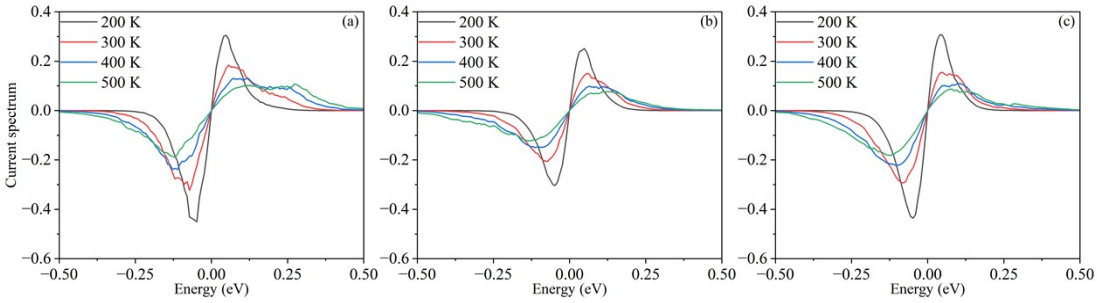

Fig. S6 The spin up current spectra for different T_L at ΔT =50 K of the Sc_2B, Ti_2B and V_2B.

The transmission spectrum, is shown the k-point averaged transmission spectrum as function of energy. The average Fermi energy of the two electrodes is set to zero. When the PDOS peaks of the left and right electrode can match each other well, there will be very large currents originating from a large transmission coefficient. Therefore, the conductance σ value is positively correlated with the transmission coefficient, as shown in Fig. S7.

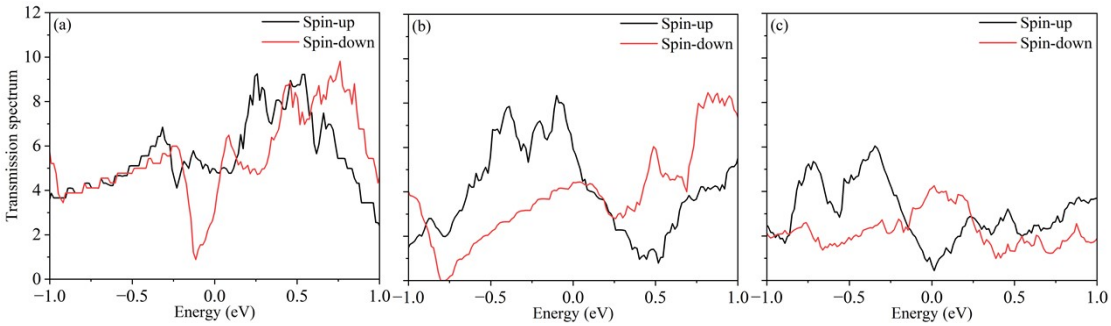

Fig. S7 The spin-dependent transmission spectrums of M_2B devices at T = 500 K. (a) Sc_2B, (b) Ti_2B, and (c) V_2B.

References

[1] Y. Imry and R. Landauer, Conductance viewed as transmission, *Rev. Mod. Phys*., 1999, **71**, S306.

[2] Y. S. Liu and Y. C. Chen, Seebeck coefficient of thermoelectric molecular junctions: First-principles calculations, *Phys. Rev. B: Condens. Matter Mater. Phys.*, 2009, **79**, 193101.

[3] B. H. Zhou, B. L. Zhou, Y. S. Zeng, M. Y. Duan and G. H. Zhou, Spin-dependent transport properties and Seebeck effects for a crossed graphene superlattice pn junction with armchair edge, *Front. Phys*., 2018, **13**, 137304.

[4] B. H. Zhou, Y. F. Gao, B. L. Zhou, Y. G. Yao, G. H. Zhou and M. Hu, Enhanced thermoelectric properties of the AGNR–GYNR heterojunctions, *Phys. Lett. A*, 2017, **381**, 3766.

[5] C. Caroli, R. Combescot, P. Nozieres, and D. Saint-James, Direct calculation of the tunneling current, *J. Phys. C: Solid State Phys.,* 1971, **4**, 916.

[6] J. Dong, B. Zhang, S. Zhang, Y. Sun and M. Long, Effects of interface charge-transfer doping on thermoelectric transport properties of black phosphorene-F4TCNQ nanoscale devices, *Appl. Surf. Sci*., 2022, **579**, 152155.

[7] C. Pan, M. Long and J. He, Enhanced thermoelectric properties in boron nitride quantum-dot, *Results Phys*., 2017, **7**, 1487–1491.

[8] X. Wu, L. Hu, D. Gu and G. Gao, Spin Transport and Spin Thermoelectric Transport in 2D Mn-Doped Blue Phosphorene with High Curie Temperature and Half-Metallicity, *J. Phys. Chem. C*, 2021, **125**, 6341–6350.